





Cite this: *Soft Matter*, 2020,  
16, 5951

Received 9th April 2020,  
Accepted 8th June 2020

DOI: 10.1039/d0sm00624f

[rsc.li/soft-matter-journal](http://rsc.li/soft-matter-journal)

# Design principles for non-reciprocal photomechanical actuation†

Markus Lahikainen,  Hao Zeng\* and Arri Priimagi  \*

Non-reciprocal motions are a sequence of movements exhibiting time-reversal asymmetry. Such movements are common among various natural species, being adopted as a typical strategy for achieving efficient locomotion. Generally, the realization of non-reciprocal motions in man-made robotic devices requires synchronous control of at least two individual actuators, hence posing challenges to soft micro-robotics where the miniaturization limits integration of different mechanical components and the possibility of using onboard batteries. Here, we introduce general concepts for achieving non-reciprocal movements in wirelessly controlled soft actuators made of photomechanically responsive liquid crystal networks. The monolithic actuators are composed of two segments that can be actuated photochemically and photothermally, and the non-reciprocal motion is obtained by a control sequence that temporally modulates light sources of different wavelengths. Through proper selection of photoactive compounds, the number of modulated light sources can be decreased, from three to two, and eventually to one. Finally, we demonstrate non-reciprocal self-oscillation by self-shadowing effect in a flexible strip under a constant light field with no temporal modulation. This study provides general guidelines to light-controlled non-reciprocal actuation, offering new strategies for the control of wireless soft micro-robotics.

## Introduction

Animals cyclically change their body shapes to generate net displacements in order to translocate their centre of mass. A typical trajectory of such movements is such that the body part deforms into a certain configuration and then returns to the original one through another sequence of motions. In other words, the motion is non-reciprocal, exhibiting time-reversal asymmetry.<sup>1</sup> Many natural species have polished the non-reciprocal movements to perfection, in order to maximize the efficiency of their motions. Fig. 1 shows a prominent example: a bird flapping its wings by following different pathways during upward and downward strokes, to produce aerodynamic forces for lifting the mass. As other examples, the tails of many fish vibrate non-reciprocally to get maximum thrust,<sup>2</sup> caterpillar squirms by following a travelling-wave-like pattern,<sup>3</sup> and bacterial flagella move non-reciprocally in low-Reynolds-number liquids.<sup>4</sup> These natural examples have inspired a significant amount of research in man-made devices, providing design tools for soft micro-robotics driven by different actuation mechanisms<sup>5–7</sup> and locomotion strategies,<sup>8,9</sup> over various dimensional scales.<sup>10–12</sup>



Fig. 1 Non-reciprocal movement of a bird. The wings flip upward and downward by following different pathways, exhibiting time-reversal asymmetry.

In principle, non-reciprocal motions in man-made devices require synchronous control of shape change of at least two individual actuators. Conventionally, this has been achieved by electronic motors/actuators synchronized by a control circuit,<sup>13</sup> or pneumatic actuators powered by a sequence of pressurized tubes.<sup>14</sup> In soft-materials-based micro-robotics, significant challenges emerge. First, miniaturization limits the overall dimensions of the device, rendering the integration of multiple electric actuators, onboard batteries, and electronic circuitry, highly complex. Second, wire-connection poses restrictions on the spaces the soft robot is able to enter and causes additional drag for the locomotion. Thus, there is a strong demand to devise stimuli-responsive materials that can replace conventional wire-based actuators for robotic motion.<sup>15–18</sup> Light-responsive liquid crystal polymer networks (LCNs) have recently emerged as

Smart Photonic Materials, Faculty of Engineering and Natural Sciences, Tampere University, P. O. Box 541, FI-33101 Tampere, Finland. E-mail: hao.zeng@tuni.fi, arri.priimagi@tuni.fi

† Electronic supplementary information (ESI) available. See DOI: 10.1039/d0sm00624f



a powerful class of materials for advanced soft actuators.<sup>19,20</sup> Through light-induced changes in molecular packing within the crosslinked network, LCNs can exhibit large deformations under moderate-intensity illumination, resulting in sophisticated control over shape changes<sup>21</sup> and, in some cases, locomotion.<sup>22,23</sup> Two distinct photomechanical effects can drive the actuation of LCNs: (i) (meta)-stable deformation *via* photochemical processes such as *cis-trans* isomerization,<sup>24–26</sup> and (ii), photothermally driven processes invoked by light-induced heat generation.<sup>27,28</sup> Utilizing these two provides great opportunities and freedom in the realization of light-fuelled soft micro-robots.<sup>29–32</sup>

Using light energy to fuel the robot has several advantages over other stimuli sources such as electric, magnetic and acoustic fields.<sup>33–36</sup> As the most significant advantage from the perspective of the present work, by selecting photoactive units with different absorption properties, one can fabricate an actuator with multiple degrees of freedom of deformation, each being controlled by different wavelength.<sup>37–39</sup> Such multi-wavelength actuation constitutes the basis for obtaining non-reciprocal movements in light-responsive LCNs. As a pioneering example, non-reciprocal movement has been obtained in printed artificial cilia composed of two LCN segments with different photomechanical properties and responding to different wavelengths of light.<sup>40</sup> Alternatively, different moving speed between two parts of the same actuator driven by the same wavelength,<sup>41</sup> or sequential deformations along the material triggered by a scanning laser beam<sup>42</sup> could also lead to non-reciprocal motions. These approaches, however, require either specific attention in material design to obtain a visible non-reciprocal pattern, or a sophisticated optical set up in order to trace the position of the object during the beam scanning. In microactuator research, there is a need to obtain non-reciprocal motion by an easily achievable optical control strategy and using easily available materials.

In this article, we report different ways of obtaining non-reciprocal movements in strip-like, photomechanical LCN actuators. The monolithic strips are made of two distinct segments that undergo photochemical and photothermal actuations. We focus on light control schemes of the simplest form: temporal modulation (on-off switching) of spatially uniform light beams. Through sequential on-off switching of different wavelengths, we invoke photochemical or photothermal actuation in different parts of the strip, and as a result, non-reciprocal motion patterns. We present a strategy to reduce the number of modulated light sources from three to two and even to one, which is important for increasing the simplicity and reducing the cost of the wireless actuation control. Finally, we demonstrate a long LCN strip that exhibits non-reciprocal self-oscillation under illumination with a constant light field. The non-reciprocal oscillation is governed by the interplay between self-shadowing effect and the flexibility of the actuating strip, yielding non-reciprocal movement without any temporal light modulation. The results presented are expected to provide new design principles for soft robotic movement and strategies of light control in future microactuator devices.

## Materials and methods

### Materials rationale

The LCN actuators are made from monomer mixtures containing liquid crystalline mesogens, photoinitiator and photo-sensitive elements (Fig. 2a). The LCNs combine liquid-crystalline order and elasticity of polymer networks, rendering the material inherently thermo-responsive, possessing the capability of reversible shape changes. We employ different photoactive units in the polymer networks to trigger actuation by different parts of the UV-visible spectrum. The absorption spectra and excitation wavelengths of the photoactive molecules used are shown in Fig. 2b and c. The azobenzene crosslinker (Fig. 2b) activates photochemical actuation and light-induced bending in response to UV irradiation *via trans-cis* isomerization, while unbending arising from *cis-trans* isomerization can be invoked with 450–500 nm irradiation. Other photoactive units employed are Disperse Red 1 (DR1) and Disperse Blue 14 (DB14), shown in Fig. 2c, which are responsible for transferring light energy into

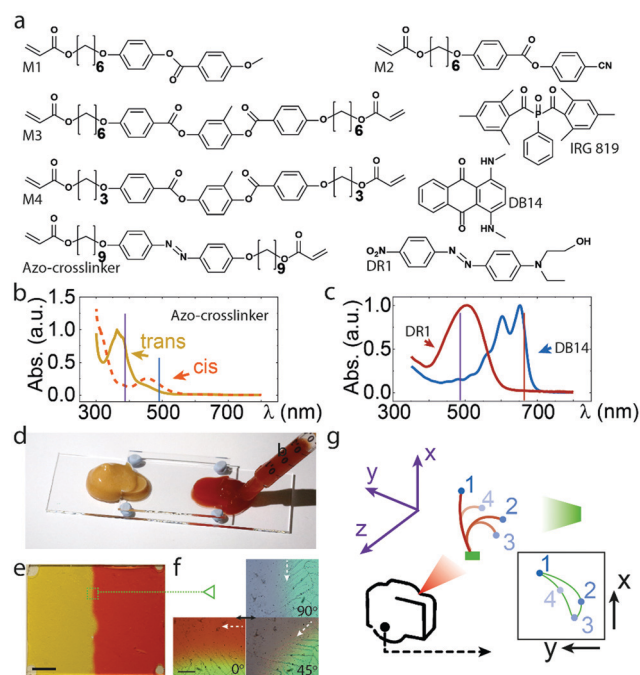


**Fig. 2** (a) Chemical structures of the molecules used to fabricate the LCNs. The LCN films contain azobenzene crosslinks (b) and light-absorbing dyes (c), which invoke photochemical and photothermal actuation, respectively. The spectra in b and c are measured from 10  $\mu\text{m}$  thick LCN films containing relevant photosensitive molecules. The vertical lines indicate the wavelengths used for excitation. (d) Illustration of the cell infiltration process for preparing the monolithic, dual-responsive photo-actuator. (e) Photograph of an LCN film with azobenzene crosslinker (left) and DR1 (right). Scale bar: 5 mm. (f) Polarized optical micrographs at different angles at the boundary between the two parts of the LCN. Scale bar: 500  $\mu\text{m}$ . The solid arrow indicates the microscope illuminating light polarization direction when arriving on the sample surface. The dashed arrow represents the alignment direction on the sample surface that is firstly exposed to the polarized light. (g) Schematic drawing of the optical setup used for tracking the non-reciprocal movements.



heat at different spectral regions, guaranteeing photothermally driven actuation alike in our previous studies.<sup>11,29</sup>

### Actuator fabrication

The monomer mixture is dissolved in dichloromethane, filtered through PTFE syringe filter (Sigma Aldrich, pore size 0.2  $\mu\text{m}$ ) and magnetically stirred at 80  $^{\circ}\text{C}$  for 2 h to remove the solvent. To make the cell, two glass slides are spin coated with polyvinyl alcohol–water solution (1 wt% PVA, Sigma Aldrich) and rubbed uni-directionally using a satin cloth. The two rubbed slides are glued together using 30  $\mu\text{m}$  spacers (silica micro-sphere, Thermo Scientific), such that the rubbing directions are aligned orthogonally with respect to each other. Such 90 $^{\circ}$  twisted alignment gives rise to unidirectional bending, irrespective of the incident light direction.<sup>43</sup> During infiltration, the cell is set on a hot plate to 95  $^{\circ}\text{C}$  (at which temperature the mixture is in the molten, isotropic state), and two different monomer mixtures are infiltrated simultaneously through the opposite edges of the cell by capillary force (Fig. 2d). After cooling down to 50  $^{\circ}\text{C}$  (3  $^{\circ}\text{C min}^{-1}$ ) to reach nematic phase, a blue LED (Prior Scientific; 420 nm, 11  $\text{mW cm}^{-2}$ , 30 min) is used to polymerize the mixture. After that, the cell is opened, and a monolithic strip actuator composed of two halves of different responsive segments is cut from the film, matching the long axis of the strip with one of the rubbing directions. The strip dimension is 15  $\times$  1  $\times$  0.03  $\text{mm}^3$ . A photograph of the resultant LCN film and polarized optical micrographs at the segment boundary are shown in Fig. 2e and f, respectively. For the self-oscillating strip, monomer mixture with DR1 is infiltrated into the glass cell with 50  $\mu\text{m}$  gap following the same procedure. The film is polymerized with 375 nm LED (Prior Scientific, 7  $\text{mW cm}^{-2}$ , 30 min) at room temperature. A strip with 20  $\times$  1  $\times$  0.05  $\text{mm}^3$  dimension is cut after opening the cell. A full list of chemical structures and composition for each fabricated actuator are given in Scheme S1 and Tables S1, S2 in ESI.<sup>†</sup>

### Optical control

LED light sources with emission wavelengths 385 nm, 490 nm and 660 nm, are coupled into a liquid light guide equipped with a collimator lens (purchased through Prior Scientific). The intensities of the light sources are 8  $\text{mW cm}^{-2}$  (385 nm), 30 or 80  $\text{mW cm}^{-2}$  (490 nm) and 100  $\text{mW cm}^{-2}$  (660 nm) measured in front of the sample. The on–off time of each LED is controlled by a hardware and synchronized by a home-made LabVIEW program. Further details on the control strategies for the different non-reciprocal actuators are compiled to Tables S3 and S4 (ESI<sup>†</sup>).

### Characterization method

The free-standing LCN strip is fixed on a support stage, and it deforms in the  $X$ – $Y$  plane, as schematically shown in Fig. 2g. The excitation light beams propagate along the  $Y$ -direction, while computer controls the sequence and timing of the light sources to be switched on and off. A camera is mounted along the  $Z$ -axis, capturing the movement of the actuator strip within the  $X$ – $Y$  plane. The photo-induced deformation is arranged to

bend towards the light source, unless mentioned otherwise. For tracking the position, a drop of fluorescent glue (containing Rhodamine 6G dyes, Merck) is used to mark the tip of the actuator. A weak UV light (365 nm, < 0.5  $\text{mW cm}^{-2}$ ; does not contribute to photochemical actuation) is used to illuminate the whole area of the sample, and the fluorescence images were captured by the camera through an optical filter cutting off wavelengths below 500 nm. The tracking position was analysed by software “Kinovea”, which extracts the trajectory during oscillation cycles, as schematically shown by the insert of Fig. 2g. The eventual trajectory pattern with non-zero area indicates the characteristic of non-reciprocal movement.

## Results and discussion

### Non-reciprocal motion *via* three-wavelength modulation

The premise for controlling two actuators (or in our case, the two parts of a monolithic LCN strip) individually upon a spatially uniform light field is that they must behave differently under identical illumination conditions. For this, we utilize the two well-recognized photomechanical actuation schemes in LCNs – the photothermal and photochemical effects. Fig. 3a

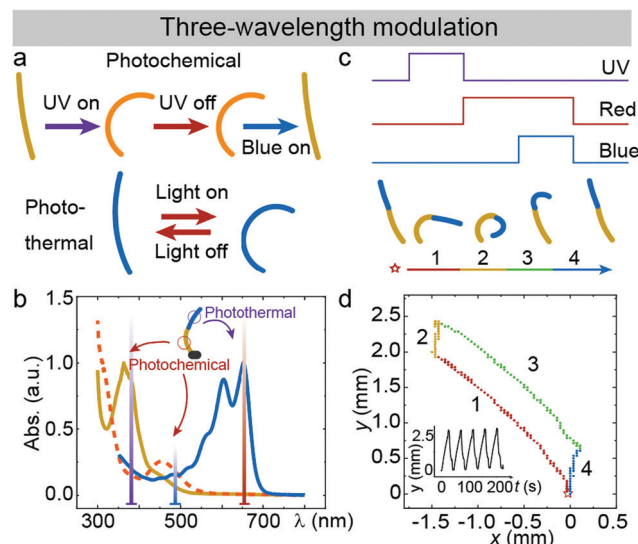


**Fig. 3** (a) Schematic illustration of the photochemical and photothermal actuation. In both cases, the bending direction is dictated by the twisted alignment and is independent of the incident light direction. (b) Absorption spectra for the two LCN segments with orthogonal photomechanical responses. The inset shows the construction of the strip, of which the photochemically activated segment (bottom part) is fixed on the stage. The vertical lines indicate the wavelengths used for exciting the two segments. (c) Light control sequence for three-wavelength modulation: (1) UV on (0 s); (2) UV off, red light on (20 s); (3) blue light on (25 s); (4) red and blue light off (35 s). Yellow and blue colors in the stripe represent azobenzene crosslinker- and DB14-containing LCN strip segments, respectively. The color scheme serves to indicate the (in-)active actuator segments at different time sequences, not representing the actual deformation in the experiment. (d) The trajectory of the strip in the  $X$ – $Y$  plane. UV: 385 nm, 8  $\text{mW cm}^{-2}$ ; blue: 490 nm, 30  $\text{mW cm}^{-2}$ ; red: 660 nm, 100  $\text{mW cm}^{-2}$ . Inset:  $Y$ -axis displacement during repeated actuation cycles. For details of chemical composition of the actuators, see Table S2 (ESI<sup>†</sup>).



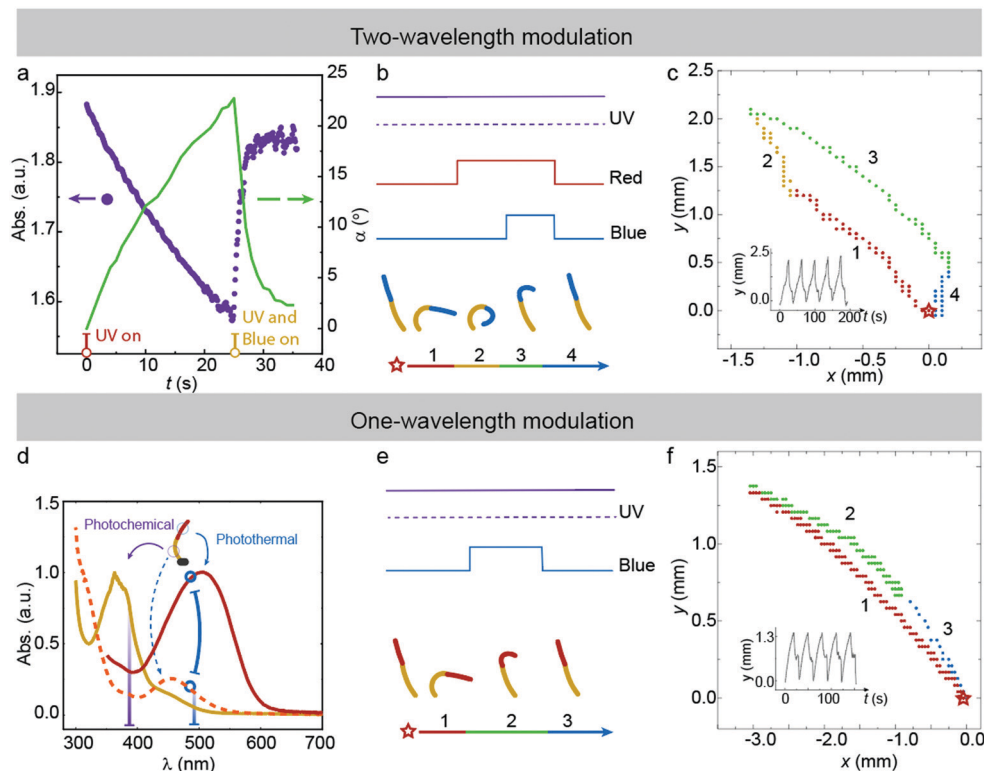
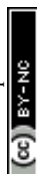


**Fig. 4** Non-reciprocal motion via two- and one-wavelength modulation. (a) Isomerization and deformation kinetics under UV and blue illumination. The isomerization kinetics was probed by monitoring the absorbance of the photochemical LCN containing azobenzene crosslinker at 400 nm, and the deformation was measured through the bending angle of the strip. (b) Light control sequence for two-wavelength modulation: (1) UV on through the entire cycle; (2) red light on (20 s); (3) blue light on (25 s); (4) red and blue light off (35 s). Yellow and blue colors in the stripe represent azobenzene crosslinker- and DB14-containing LCN segments, respectively. (c) The trajectory of the strip in the  $X$ - $Y$  plane, indicating non-reciprocal movement. UV: 385 nm, 8 mW cm<sup>-2</sup>; blue: 490 nm, 80 mW cm<sup>-2</sup>; red: 660 nm, 100 mW cm<sup>-2</sup>. Inset:  $Y$ -axis displacement during repeated actuation cycles. (d) The overlapping absorption bands of the  $n$ - $\pi^*$  transition of the azobenzene crosslinks in one segment, and the  $\pi$ - $\pi^*$  transition of DR1 in the other segment. Inset shows the construction of strip containing two individual segments, where the photochemical segment is fixed on the stage. The vertical lines indicate the wavelengths used for excitation. (e) Light control sequence for one-wavelength modulation: (1) UV on throughout the entire cycle; (2) blue light on (20 s); (3) blue light off (30 s). Yellow and red colors represent azobenzene crosslinker- and DR1-containing LCN strip segments, respectively. (f) The trajectory of the strip in the  $X$ - $Y$  plane. UV: 385 nm, 8 mW cm<sup>-2</sup>; blue: 490 nm, 80 mW cm<sup>-2</sup>. Inset:  $Y$ -axis displacement during repeated actuation cycles. The color scheme in (b) and (e) serve to indicate the (in-)active actuator segments at different time sequences, not representing the actual deformation in the experiment. For details of chemical composition of the actuators, see Table S2 (ESI†).

schematically illustrates the differences between these two actuation modes. Photochemical actuation is based on *trans*-*cis* isomerization of azobenzene crosslinks, typically induced with UV light, which creates inner stress into the LCN to yield macroscopic deformation.<sup>44</sup> The deformation can sustain for a time period ranging from few minutes to several days after ceasing the UV illumination, depending on the *cis*-lifetime of the azobenzene used.<sup>45,46</sup> Alternatively, the original state can be retained using blue light to induce *cis*-*trans* isomerization. The photothermal effect is triggered by light-absorbing moieties (DR1 or DB14 dyes in our case) incorporated into the LCN, which convert the energy from absorbed photons into heat.<sup>47,48</sup> Heat causes the inner stress required for macroscopic deformation, which vanishes once the irradiation is ceased.

We fabricated an LCN actuator with two segments, one comprising the azobenzene crosslinks to invoke the photochemical effect, and the other with DB14 for triggering the photothermal effect. Fig. 3b shows the absorption spectra of

the two segments. Their activation wavelengths are well separated, allowing orthogonal control of the lower and upper parts of the actuator. Non-reciprocal motion can be obtained by the light control sequence depicted in Fig. 3c: (1) UV light on  $\rightarrow$  the bottom part bends; (2) UV light off  $\rightarrow$  the bottom part remains bent & red light on  $\rightarrow$  the upper part bends; (3) blue light on  $\rightarrow$  the bottom part unbends while the upper part remains bent; (4) red light off  $\rightarrow$  the upper part unbends & blue light off  $\rightarrow$  the system resets and a new cycle can start. The trajectory pattern in the  $X$ - $Y$  plane is shown in Fig. 3d, indicating a clear non-reciprocal behaviour. Conversely, both photochemical and photothermal actuation modes separately lead to reciprocal motion, in which case the strip deforms and relaxes *via* the same path, as illustrated in Fig. S1 (ESI†). By repeating the light control sequence depicted in Fig. 3c, a cyclic non-reciprocal motion is obtained. The consistence between several successive actuation cycles is shown by the  $Y$ -axis displacement data, given in the inset of Fig. 3d.



### Non-reciprocal motion via two-wavelength modulation

To reduce the number of light beams to be modulated, we use a strategy that makes use of different kinetics of photoinduced *trans-cis* and *cis-trans* isomerization of the azobenzene crosslinker. Fig. 4a shows the absorbance change and deformation kinetics of the LCN upon photochemical activation. Under UV irradiation ( $8 \text{ mW cm}^{-2}$ ), the azobenzene crosslinks undergo *trans-cis* isomerization, giving rise to a decrease in the absorbance of the  $\pi\text{-}\pi^*$  band. Within 25 s, approximately 15% of the azobenzenes isomerize to the *cis*-state. By switching on the blue light ( $80 \text{ mW cm}^{-2}$ ) while maintaining the UV illumination, the absorbance rapidly recovers with a time constant of 1.2 s and saturates at a value slightly below the initial absorbance. From this we can deduce that the photostationary state upon simultaneous UV and blue irradiation comprises *ca.* 97% *trans*-isomers. The kinetics of absorbance change is in line with the photomechanical actuation: the strip bends slowly upon UV irradiation and rapidly unbends when the blue light is switched on. These observations indicate that photochemical *cis-trans* isomerization is the dominating effect when the actuator is activated within UV + blue spectral range.

The non-reciprocal motion using two-wavelength modulation can be obtained with the same actuator strip as was used for three-wavelength modulation, using the light control sequence shown in Fig. 4b: (1) for the entire cycle, UV light is on  $\rightarrow$  the bottom part bends; (2) red light on  $\rightarrow$  the upper part bends, while the bottom part remains bent; (3) blue light on  $\rightarrow$  the bottom part unbends, while the upper part remains bent as the red light is on; (4) red light off  $\rightarrow$  the upper part relaxes; the system resets when the blue light is ceased and a new cycle can start. The non-reciprocal behavior is shown by the *X-Y* trajectory pattern in Fig. 4c, while the inset of Fig. 4c confirms the repeatability of the cyclic actuation. Finally, we note that a strip composed of two segments that can be photothermally activated at different wavelengths can also perform non-reciprocal movements, as detailed in Fig. S2 (ESI<sup>†</sup>).

### Non-reciprocal motion via one-wavelength modulation

To further reduce the number of modulating light beams, an overlap between the absorption bands that trigger *cis-trans* isomerization of the azobenzene crosslinks and the photothermal actuation in a different segment of the LCN strip, is adopted and illustrated in Fig. 4d. Hence, we invoke the photochemical *cis-trans* isomerization and the photothermal effect simultaneously with a single wavelength (490 nm), causing the different segments of the strip to bend (photothermal activation) and unbend (photochemical activation). We note that the photothermal dye used, DR1, also undergoes photoisomerization, but when doped to LCN, the actuation arises solely from the photothermal effect.<sup>49</sup> The following light control sequence is used (Fig. 4e): (1) for the entire cycle, UV light is on  $\rightarrow$  the bottom part bends (20 s); (2) blue light on  $\rightarrow$  the bottom part unbends and at the same time, the upper part bends; (3) blue light off  $\rightarrow$  the upper part unbends, the system resets and a new cycle can start. The non-reciprocal trajectory

pattern is shown in Fig. 4f, and the *Y*-axis displacement is again used to monitor the reversibility of the actuation cycles (inset of Fig. 4f).

### Non-reciprocal self-oscillation

To obtain non-reciprocal self-oscillation with spatially and temporally constant laser illumination (which we denote as zero-wavelength modulation in Fig. 5), the movement of the actuator should not only be non-reciprocal, but also cyclic and self-sustained.<sup>50</sup> Self-oscillation has been widely studied among light-driven actuators.<sup>47,51–58</sup> Most of the studies employ bending strips, however, non-reciprocal self-oscillation has rarely been reported.<sup>52,54</sup> Self-shadowing is an intriguing concept for achieving self-oscillation, which has been utilized in wave-like motion (a symbol of non-reciprocal motion) and autonomous locomotion in LCNs.<sup>54</sup>

We employ a strategy built on the combination of the self-shadowing effect and flexibility of the actuator body in a long, free-standing LCN strip. A continuous-wave 532 nm laser beam is used to excite the strip along horizontal direction (Fig. 5a), and the oscillation kinetics is followed to confirm the non-reciprocal motion. The monolithic strip can be divided into two parts, marked as A and B in Fig. 5a(i). Part B is defined by the area where the incident beam firstly hits, *i.e.*, it is confined close to the base the actuator is attached to. The rest of the strip forms Part A. Even if the chemical composition (Table S2, ESI<sup>†</sup>) of the two parts is identical, Part A dictates the photodeformation, yielding a dynamic change of centre of mass of the strip

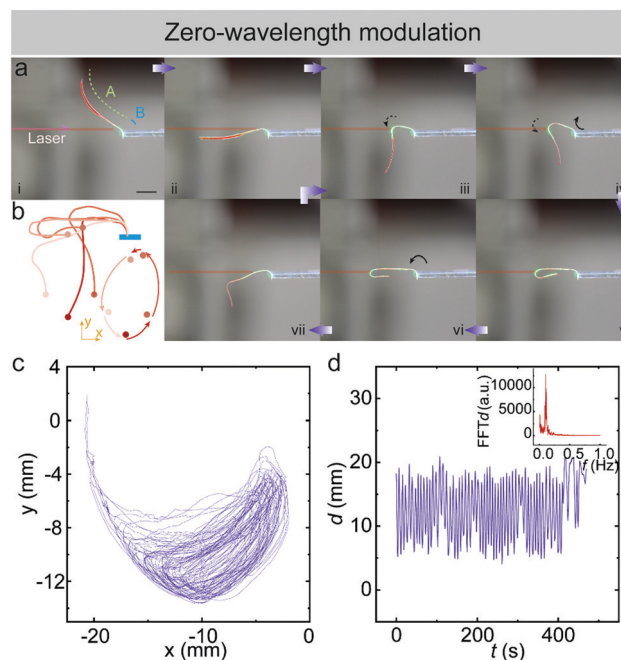


**Fig. 5** Non-reciprocal self-oscillation. (a) Optical images of LCN self-oscillator under a constant laser beam excitation. Scale bar: 5 mm. Laser beam, 532 nm, 100 mW. Spot diameter: 2 mm. (b) Schematic drawing of the principle of oscillating kinetics. (c) *X-Y* movement trajectory of the trip position in 50 oscillation cycles. (d) Tip displacement during sequent oscillating cycles. Inset shows the Fourier transform of displacement data.



and the torque imposed on Part B due to the gravity, while Part B is responsible for mechanical relaxation but does not directly contribute to the cyclic photomechanical actuation. Any change in torque or modulus of the strip leads to bending of Part B in either clockwise or anticlockwise direction. When the laser beam is exciting Part B, it bends anticlockwise, causing Part A to shadow Part B (Fig. 5a(ii); Movie S1, ESI†). From thereon, only Part A is exposed to laser excitation. Fig. S3 (ESI†) presents top-view and bottom-view images of the LCN strip during the oscillation cycles.

The self-oscillation process is promoted by the following steps: initially, the beam hits Part A at the “bottom”, *i.e.*, close to where it meets Part B (Fig. 5a(iii)). The photoinduced bending of the strip leads to a reduced torque raised by the gravity of Part A, and at the same time, the stiffness of Part B rebounds the cantilever by slightly bending to the clockwise direction (iv). This movement raises the height of Part A and brings about a continuous change of the spot where the laser hits the cantilever and hence its shape (iv–v–vi). While the cantilever is extending towards left (vi), the gravity-induced torque in Part A increases, forcing Part B to bend anticlockwise. The bending of Part B, in turn, reduces the height of Part A, allowing the incident beam to reach the “bottom” of Part A again (vii). At the same time, the deformed portion of Part A relaxes while the “bottom” of Part A starts to photodeform (vii-to-iii), and a new cycle can begin. The movement trajectory clearly exhibits a non-reciprocal pattern in the *X–Y* plane, as illustrated in Fig. 5b. Fig. 5c presents the evolution of *X–Y* plane trajectory over *ca.* 50 oscillation cycles. For more details, see the *X–Y* trajectory evolution data in Fig. S4 and Movie S2 (ESI†). The fact that subsequent trajectories follow different paths most likely arises from slight irreversibility in the properties of the polymer network upon photoactuation. However, the oscillation can self-sustain over extended periods of time, as confirmed by monitoring the oscillation of the strip over a time span of 400 s (Fig. 5d and Fig. S5, ESI†). The oscillation frequency is around 0.1 Hz, as indicated by the Fourier transform data shown in the inset of Fig. 5d.

## Discussion

The non-reciprocal trajectory is sensitive to the experimental arrangement, *i.e.*, the positions of the two segments and their related deformation. For instance, reversing the photothermal and photochemical segments, such that the former is positioned to the bottom, or flipping the strip to reverse its bending direction, yield different non-reciprocal trajectories as illustrated in Fig. S6 and S7 (ESI†). Changing the ratio between the length of the photothermal and photochemical segments varies the pattern of the trajectory, yet the motion remains non-reciprocal (Fig. S8, ESI†). The efficiency of non-reciprocal motion, which can be visualized by the loop area under the *X–Y* trajectory within one oscillating cycle (*e.g.* Fig. 3d, 4c, f and 5c), can be improved by separately optimizing the deformation of each part of the actuator. More importantly, orthogonality of actuation, *i.e.*, separate addressability of the actuator segments, plays a significant role. For example, upon the three- and two-wavelength

modulation strategies, spectral separation allows individual control between the photochemically and photothermally actuated parts, yielding large non-reciprocal movement (Fig. 3d and 4c). However, when the two parts cross-talk, which is the case for the one-wavelength modulation strategy, the photochemical relaxation (unbending) and photothermal actuation occur simultaneously, yielding only minor non-reciprocal motion as observed in Fig. 4f.

It is important to study how to translate the cyclic movement of an actuator into robotic locomotion.<sup>59,60</sup> Along this direction, many pioneering results have been reported. To achieve walking on a surface, the conventional approach leans on friction bias during the cyclic deformation.<sup>25,61</sup> Non-reciprocal motion allows, for instance, a travelling-wave-like motion to induce locomotion without the need for friction asymmetry at the robot–substrate interface.<sup>62,63</sup> Non-reciprocal motion has also been exploited in creating micro-swimmers, especially in low-Reynolds-number liquids.<sup>64–66</sup> However, underwater actuation is hindered by quick heat dissipation in aqueous environment, rendering photothermal processes inefficient. Recent study on underwater actuation using liquid-crystal gels addressed this problem, pointing a way forward for underwater self-oscillation.<sup>67</sup>

To meet the capacities required for flying, the non-reciprocal motion speed has to be boosted in order to produce sufficient air thrust. At the same time, the density of the actuating device should be minimized. To meet those requirements, great effort has been recently dedicated towards improving the material properties, *e.g.*, the use of chain extenders to enhance the deformability,<sup>68,69</sup> and interpenetrating networks to increase the robustness.<sup>70</sup> Reconfigurability and programmability of the motions are also important in view of increasing the versatility of photoinduced motions.<sup>71–73</sup> These will lead to ever-more advanced robot realizations and non-reciprocal motions in the near future.

## Conclusions

Different light-control strategies have been introduced to achieve non-reciprocal movements in photomechanical liquid-crystal network (LCN) actuators. By proper selection of the photoactive moieties, photochemical and photothermal actuation can be induced separately in two distinct segments of a monolithic LCN strip. Specific light control sequences, based on three-, two-, and one-wavelength modulation, are designed to bring about non-reciprocal motions. Finally, a non-reciprocal self-oscillator is demonstrated in a free-standing LCN strip. This actuator can sustain the non-reciprocal motion upon a spatially and temporally constant light field, benefitting from self-shadowing and the flexibility of the long, strip-like structure. The results provide general guidelines to simplify the modulation of the light fields, offering design principles for complex and non-reciprocal light-controlled movements and alternatives for wireless soft robotics.

## Conflicts of interest

There are no conflicts to declare.



## Acknowledgements

The work is supported by the European Research Council (Starting Grant PHOTOTUNE, Agreement No. 679646) and the Academy of Finland (the Flagship Programme on Photonics Research and Innovation, PREIN, no. 320165, and a postdoctoral grant no. 316416). ML is thankful for the Emil Aaltonen Foundation for the funding support (Grant number 190113 N1).

## References

- 1 M. H. Dickinson, C. T. Farley, R. J. Full, M. A. R. Koehl, R. Kram and S. Lehman, *Science*, 2000, **288**, 100–106.
- 2 M. Sfakiotakis, D. M. Lane and J. B. C. Davies, *IEEE J. Oceanic Eng.*, 1999, **24**, 237–252.
- 3 L. I. van Griethuijsen and B. A. Trimmer, *Biol. Rev.*, 2014, **89**, 656–670.
- 4 E. M. Purcell, *Am. J. Phys.*, 1977, **45**, 3–11.
- 5 W. Hu, G. Z. Lum, M. Mastrangeli and M. Sitti, *Nature*, 2018, **554**, 81–85.
- 6 M. Wehner, R. L. Truby, D. J. Fitzgerald, B. Mosadegh, G. M. Whitesides, J. A. Lewis and R. J. Wood, *Nature*, 2016, **536**, 451–455.
- 7 C. Laschi, B. Mazzolai and M. Cianchetti, *Sci. Robot.*, 2016, **1**, aah3690.
- 8 K. Ma, P. Chirarattananon, S. Fuller and R. J. Wood, *Science*, 2013, **340**, 603–607.
- 9 Y. Wu, J. K. Yim, J. Liang, Z. Shao, M. Qi, J. Zhong, Z. Luo, X. Yan, M. Zhang, X. Wang, R. S. Fearing, R. J. Full and L. Lin, *Sci. Robot.*, 2019, **4**, eaax1594.
- 10 D. Martella, S. Nocentini, D. Nuzhdin, C. Parmeggiani and D. S. Wiersma, *Adv. Mater.*, 2017, **29**, 1704047.
- 11 O. M. Wani, H. Zeng and A. Priimagi, *Nat. Commun.*, 2017, **8**, 15546.
- 12 E. Diller and M. Sitti, *Adv. Funct. Mater.*, 2014, **24**, 4397–4404.
- 13 P. Liljebck, K. Y. Pettersen, O. Stavadahl and J. T. Gravdahl, *Robot. Auton. Syst.*, 2012, **60**, 29–40.
- 14 R. F. Shepherd, F. Ilievski, W. Choi, S. A. Morin, A. A. Stokes, A. D. Mazzeo, X. Chen, M. Wang and G. M. Whitesides, *Proc. Natl. Acad. Sci. U. S. A.*, 2011, **108**, 20400–20403.
- 15 D. Rus and M. T. Tolley, *Nature*, 2015, **521**, 467–475.
- 16 L. Hines, K. Petersen, G. Z. Lum and M. Sitti, *Adv. Mater.*, 2017, **29**, 1603483.
- 17 S. Kim, C. Laschi and B. Trimmer, *Trends Biotechnol.*, 2013, **31**, 287–294.
- 18 J. M. McCracken, B. R. Donovan and T. J. White, *Adv. Mater.*, 2020, **32**, 1906564.
- 19 J. del Barrio and C. Sánchez-Somolinos, *Adv. Opt. Mater.*, 2019, **7**, 1900598.
- 20 H. Zeng, P. Wasylczyk, D. S. Wiersma and A. Priimagi, *Adv. Mater.*, 2018, **30**, 1703554.
- 21 T. Ube and T. Ikeda, *Adv. Opt. Mater.*, 2019, **7**, 1900380.
- 22 M. Pilz da Cunha, S. Ambergen, M. G. Debije, E. F. G. A. Homburg, J. M. J. den Toonder and A. P. H. J. Schenning, *Adv. Sci.*, 2020, **7**, 1902842.
- 23 L. Dong, X. Tong, H. Zhang, M. Chen and Y. Zhao, *Mater. Chem. Front.*, 2018, **2**, 1383–1388.
- 24 F. Lancia, A. Ryabchun and N. Katsonis, *Nat. Rev. Chem.*, 2019, **3**, 536–551.
- 25 M. Yamada, M. Kondo, R. Miyasato, Y. Naka, J. I. Mamiya, M. Kinoshita, A. Shishido, Y. Yu, C. J. Barrett and T. Ikeda, *J. Mater. Chem.*, 2009, **19**, 60–62.
- 26 S. K. Ahn, T. H. Ware, K. M. Lee, V. P. Tondiglia and T. J. White, *Adv. Funct. Mater.*, 2016, **26**, 5819–5826.
- 27 L. Liu, M. H. Liu, L. L. Deng, B. P. Lin and H. Yang, *J. Am. Chem. Soc.*, 2017, **139**, 11333–11336.
- 28 Y. Hu, Z. Li, T. Lan and W. Chen, *Adv. Mater.*, 2016, **28**, 10548–10556.
- 29 M. Lahikainen, H. Zeng and A. Priimagi, *Nat. Commun.*, 2018, **9**, 4148.
- 30 Z. Cheng, T. Wang, X. Li, Y. Zhang and H. Yu, *ACS Appl. Mater. Interfaces*, 2015, **7**, 27494–27501.
- 31 C. Huang, J. A. Lv, X. Tian, Y. Wang, Y. Yu and J. Liu, *Sci. Rep.*, 2015, **5**, 17414.
- 32 H. Zeng, P. Wasylczyk, C. Parmeggiani, D. Martella, M. Burrese and D. S. Wiersma, *Adv. Mater.*, 2015, **27**, 3883–3887.
- 33 M. Sitti and D. S. Wiersma, *Adv. Mater.*, 2020, 1906766.
- 34 I. A. Anderson, T. A. Gisby, T. G. McKay, B. M. O'Brien and E. P. Calius, *J. Appl. Phys.*, 2012, **112**, 041101.
- 35 T. Qiu, S. Palagi, A. G. Mark, K. Melde, F. Adams and P. Fischer, *Appl. Phys. Lett.*, 2016, **109**, 191602.
- 36 Q. He, Z. Wang, Y. Wang, A. Minori, M. T. Tolley and S. Cai, *Sci. Adv.*, 2019, **5**, eaax5746.
- 37 B. Zuo, M. Wang, B. P. Lin and H. Yang, *Nat. Commun.*, 2019, **10**, 4539.
- 38 A. H. Gelebart, D. J. Mulder, G. Vantomme, A. P. H. J. Schenning and D. J. Broer, *Angew. Chem., Int. Ed.*, 2017, **56**, 13436–13439.
- 39 M. Wang, Y. Han, L. X. Guo, B. P. Lin and H. Yang, *Liq. Cryst.*, 2019, **46**, 1231–1240.
- 40 C. L. Van Oosten, C. W. M. Bastiaansen and D. J. Broer, *Nat. Mater.*, 2009, **8**, 677–682.
- 41 D. Martella, D. Antonioli, S. Nocentini, D. S. Wiersma, G. Galli, M. Laus and C. Parmeggiani, *RSC Adv.*, 2017, **7**, 19940–19947.
- 42 S. Palagi, A. G. Mark, S. Y. Reigh, K. Melde, T. Qiu, H. Zeng, C. Parmeggiani, D. Martella, A. Sanchez-Castillo, N. Kapernaum, F. Giesselmann, D. S. Wiersma, E. Lauga and P. Fischer, *Nat. Mater.*, 2016, **15**, 647–653.
- 43 C. L. Van Oosten, K. D. Harris, C. W. M. Bastiaansen and D. J. Broer, *Eur. Phys. J. E: Soft Matter Biol. Phys.*, 2007, **23**, 329–336.
- 44 M. Yamada, M. Kondo, J. I. Mamiya, Y. Yu, M. Kinoshita, C. J. Barrett and T. Ikeda, *Angew. Chem., Int. Ed.*, 2008, **47**, 4986–4988.
- 45 M. Pilz Da Cunha, E. A. J. Van Thoor, M. G. Debije, D. J. Broer and A. P. H. J. Schenning, *J. Mater. Chem. C*, 2019, **7**, 13502–13509.
- 46 S. Iamsaard, E. Anger, S. J. Afshoff, A. Depauw, S. P. Fletcher and N. Katsonis, *Angew. Chem., Int. Ed.*, 2016, **55**, 9908–9912.
- 47 A. H. Gelebart, G. Vantomme, B. E. W. Meijer and D. J. Broer, *Adv. Mater.*, 2017, **29**, 1606712.



- 48 Z. Wang, K. Li, Q. He and S. Cai, *Adv. Mater.*, 2019, **31**, 1806849.
- 49 H. Zeng, O. M. Wani, P. Wasylczyk, R. Kaczmarek and A. Priimagi, *Adv. Mater.*, 2017, **29**, 1701814.
- 50 A. Jenkins, *Phys. Rep.*, 2013, **525**, 167–222.
- 51 T. J. White, N. V. Tabiryan, S. V. Serak, U. A. Hrozhyk, V. P. Tondiglia, H. Koerner, R. A. Vaia and T. J. Bunning, *Soft Matter*, 2008, **4**, 1796–1798.
- 52 H. Zeng, M. Lahikainen, L. Liu, Z. Ahmed, O. M. Wani, M. Wang, H. Yang and A. Priimagi, *Nat. Commun.*, 2019, **10**, 5057.
- 53 F. Ge and Y. Zhao, *Chem. Sci.*, 2017, **8**, 6307–6312.
- 54 A. H. Gelebart, D. J. Mulder, M. Varga, A. Konya and G. Vantomme, *Nature*, 2017, **546**, 632–636.
- 55 R. Lan, J. Sun, C. Shen, R. Huang, Z. Zhang, L. Zhang, L. Wang and H. Yang, *Adv. Mater.*, 2020, **32**, 1906319.
- 56 G. Vantomme, A. H. Gelebart, D. J. Broer and E. W. Meijer, *Tetrahedron*, 2017, **73**, 4963–4967.
- 57 K. M. Lee, M. L. Smith, H. Koerner, N. Tabiryan, R. A. Vaia, T. J. Bunning and T. J. White, *Adv. Funct. Mater.*, 2011, **21**, 2913–2918.
- 58 Y. Kageyama, *ChemPhotoChem*, 2019, **3**, 327–336.
- 59 C. Ahn, K. Li and S. Cai, *ACS Appl. Mater. Interfaces*, 2018, **10**, 25689–25696.
- 60 J. J. Wie, M. R. Shankar and T. J. White, *Nat. Commun.*, 2016, **7**, 13260.
- 61 H. Zeng, O. M. Wani, P. Wasylczyk and A. Priimagi, *Macromol. Rapid Commun.*, 2017, **39**, 201700224.
- 62 M. Rogóż, K. Dradrach, C. Xuan and P. Wasylczyk, *Macromol. Rapid Commun.*, 2019, **40**, 1970036.
- 63 M. Rogóż, H. Zeng, C. Xuan, D. S. Wiersma and P. Wasylczyk, *Adv. Opt. Mater.*, 2016, **4**, 1689–1694.
- 64 S. Tottori, L. Zhang, F. Qiu, K. K. Krawczyk, A. Franco-Obregón and B. J. Nelson, *Adv. Mater.*, 2012, **24**, 811–816.
- 65 H. Zhang, L. Koens, E. Lauga, A. Mourran and M. Möller, *Small*, 2019, **15**, 1903379.
- 66 A. M. Maier, C. Weig, P. Oswald, E. Frey, P. Fischer and T. Liedl, *Nano Lett.*, 2016, **16**, 906–910.
- 67 H. Shahsavan, A. Aghakhani, H. Zeng, Y. Guo, Z. S. Davidson, A. Priimagi and M. Sitti, *Proc. Natl. Acad. Sci. U. S. A.*, 2020, **117**, 5125–5133.
- 68 H. H. Yoon, D. Y. Kim, K. U. Jeong and S. K. Ahn, *Macromolecules*, 2018, **51**, 1141–1149.
- 69 T. H. Ware, M. E. McConney, J. J. Wie, V. P. Tondiglia and T. J. White, *Science*, 2015, **347**, 982–984.
- 70 H.-F. Lu, M. Wang, X.-M. Chen, B.-P. Lin and H. Yang, *J. Am. Chem. Soc.*, 2019, **141**, 14364–14369.
- 71 Y. Yang, E. M. Terentjev, Y. Wei and Y. Ji, *Nat. Commun.*, 2018, **9**, 1906.
- 72 T. Ube, K. Kawasaki and T. Ikeda, *Adv. Mater.*, 2016, **28**, 8212–8217.
- 73 Z. Wang, H. Tian, Q. He and S. Cai, *ACS Appl. Mater. Interfaces*, 2017, **9**, 33119–33128.

